J|A|C|S
ARTICLES
Published on Web 12/15/2006

Catalyst-Assisted Solution−Liquid−Solid Synthesis of CdS/CdSe Nanorod Heterostructures

Lian Ouyang, Kristin N. Maher, Chun Liang Yu, Justin McCarty, and Hongkun Park*
Contribution from the Department of Chemistry and Chemical Biology, Harvard University, 12 Oxford Street, Cambridge, Massachusetts 02138

Received August 28, 2006; E-mail: Hongkun_Park@harvard.edu

Abstract: We report the synthesis and characterization of axial nanorod heterostructures composed of cadmium selenide (CdSe) and cadmium sulfide (CdS). The synthesis employs a solution−liquid−solid (SLS) mechanism with the assistance of bismuth nanocrystals adhered to a substrate (silicon or a III−V semiconductor). Transmission electron microscopy (TEM) and diffraction studies show that CdSe and CdS segments exhibit the wurtzite (hexagonal) crystal structure with <5% stacking faults. Both of these segments grow along the [002] direction with an epitaxial interface between them. Energy-dispersive X-ray (EDX) spectrometry using a high-resolution TEM operating in scanning mode confirms the alloy-free composition modulation in the nanorod heterostructures, showing that Se and S are localized in the CdSe and CdS portions of the nanorod heterostructures, respectively. This study demonstrates that SLS synthesis provides an alternate route to prepare axial nanorod heterostructures that have been difficult to generate using either vapor−liquid−solid growth or catalyst-free solution-phase synthesis.

Introduction

Over the past decade, one-dimensional (1D) inorganic nanostructures have emerged as promising materials for fundamental studies and possible technological applications.[1−20] These structures exhibit physical and chemical properties distinct from their bulk counterparts due to radial confinement, while they retain the advantages of wirelike connectivity. In particular, semiconductor-based 1D nanostructures have been the subject of numerous research activities[1−7,9−11] and have been used to realize prototype electrical,[15,16] optical,[17,18] and optoelectronic[19,20] device test beds.

More recently, the preparation of nanorods and nanowires with axially and radially modulated compositions has led to further scientific and technological development.[21−35] Akin to the layer-by-layer band gap engineering in thin-film semiconductor heterostructures, these nanowire and nanorod heterostructures have the potential to revolutionize nanomaterial research by providing means to define multiple functionalities within a single nanostructure. Various device functionalities exploiting the unique properties of 1D heterostructures have already been demonstrated, including single-electron transis-

(1) Hu, J. T.; Odom, T. W.; Lieber, C. M. *Acc. Chem. Res.* **1999**, *32*, 435−445.
(2) Law, M.; Goldberger, J.; Yang, P. D. *Annu. Rev. Mater. Res.* **2004**, *34*, 83−122.
(3) Pan, Z. W.; Dai, Z. R.; Wang, Z. L. *Science* **2001**, *291*, 1947−1949.
(4) Wang, Z. L. *Nanowires and Nanobelts*; Kluwer Academic Publisher: New York, 2003.
(5) Xia, Y. N.; Yang, P. D.; Sun, Y. G.; Wu, Y. Y.; Mayers, B.; Gates, B.; Yin, Y. D.; Kim, F.; Yan, Y. Q. *Adv. Mater.* **2003**, *15*, 353−389.
(6) Morales, A. M.; Lieber, C. M. *Science* **1998**, *279*, 208−211.
(7) Persson, A. I.; Larsson, M. W.; Stenstrom, S.; Ohlsson, B. J.; Samuelson, L.; Wallenberg, L. R. *Nat. Mater.* **2004**, *3*, 677−681.
(8) Peng, X. G.; Manna, L.; Yang, W. D.; Wickham, J.; Scher, E.; Kadavanich, A.; Alivisatos, A. P. *Nature* **2000**, *404*, 59−61.
(9) Peng, Z. A.; Peng, X. G. *J. Am. Chem. Soc.* **2002**, *124*, 3343−3353.
(10) Manna, L.; Scher, E. C.; Alivisatos, A. P. *J. Am. Chem. Soc.* **2000**, *122*, 12700−12706.
(11) Barrelet, C. J.; Wu, Y.; Bell, D. C.; Lieber, C. M. *J. Am. Chem. Soc.* **2003**, *125*, 11498−11499.
(12) Urban, J. J.; Yun, W. S.; Gu, Q.; Park, H. *J. Am. Chem. Soc.* **2002**, *124*, 1186−1187.
(13) Guiton, B. S.; Gu, Q.; Prieto, A. L.; Gudiksen, M. S.; Park, H. *J. Am. Chem. Soc.* **2005**, *127*, 498−499.
(14) Ouyang, L.; Thrall, E. S.; Deshmukh, M. M.; Park, H. *Adv. Mater.* **2006**, *18*, 1437−1440.
(15) Huang, Y.; Duan, X. F.; Cui, Y.; Lauhon, L. J.; Kim, K. H.; Lieber, C. M. *Science* **2001**, *294*, 1313−1317.
(16) Goldberger, J.; Hochbaum, A. I.; Fan, R.; Yang, P. D. *Nano Lett.* **2006**, *6*, 973−977.
(17) Kazes, M.; Lewis, D. Y.; Ebenstein, Y.; Mokari, T.; Banin, U. *Adv. Mater.* **2002**, *14*, 317−321.
(18) Huynh, W. U.; Dittmer, J. J.; Alivisatos, A. P. *Science* **2002**, *295*, 2425−2427.
(19) Duan, X. F.; Huang, Y.; Agarwal, R.; Lieber, C. M. *Nature* **2003**, *421*, 241−245.
(20) Gudiksen, M. S.; Maher, K. N.; Ouyang, L.; Park, H. *Nano Lett.* **2005**, *5*, 2257−2261.
(21) Bjork, M. T.; Ohlsson, B. J.; Sass, T.; Persson, A. I.; Thelander, C.; Magnusson, M. H.; Deppert, K.; Wallenberg, L. R.; Samuelson, L. *Appl. Phys. Lett.* **2002**, *80*, 1058−1060.
(22) Thelander, C.; Martensson, T.; Bjork, M. T.; Ohlsson, B. J.; Larsson, M. W.; Wallenberg, L. R.; Samuelson, L. *Appl. Phys. Lett.* **2003**, *83*, 2052−2054.
(23) Gudiksen, M. S.; Lauhon, L. J.; Wang, J.; Smith, D. C.; Lieber, C. M. *Nature* **2002**, *415*, 617−620.
(24) Yang, C.; Zhong, Z. H.; Lieber, C. M. *Science* **2005**, *310*, 1304−1307.
(25) Solanki, R.; Huo, J.; Freeouf, J. L.; Miner, B. *Appl. Phys. Lett.* **2002**, *81*, 3864−3866.
(26) Wu, Y. Y.; Fan, R.; Yang, P. D. *Nano Lett.* **2002**, *2*, 83−86.
(27) Xiang, J.; Lu, W.; Hu, Y. J.; Wu, Y.; Yan, H.; Lieber, C. M. *Nature* **2006**, *441*, 489−493.
(28) Lauhon, L. J.; Gudiksen, M. S.; Wang, C. L.; Lieber, C. M. *Nature* **2002**, *420*, 57−61.
(29) Qian, F.; Li, Y.; Gradecak, S.; Wang, D. L.; Barrelet, C. J.; Lieber, C. M. *Nano Lett.* **2004**, *4*, 1975−1979.
(30) Wu, Y.; Xiang, J.; Yang, C.; Lu, W.; Lieber, C. M. *Nature* **2004**, *430*, 61−65.
(31) Milliron, D. J.; Hughes, S. M.; Cui, Y.; Manna, L.; Li, J. B.; Wang, L. W.; Alivisatos, A. P. *Nature* **2004**, *430*, 190−195.
(32) Shieh, F.; Saunders, A. E.; Korgel, B. A. *J. Phys. Chem. B* **2005**, *109*, 8538−8542.
(33) Talapin, D. V.; Koeppe, R.; Gotzinger, S.; Kornowski, A.; Lupton, J. M.; Rogach, A. L.; Benson, O.; Feldmann, J.; Weller, H. *Nano Lett.* **2003**, *3*, 1677−1681.
(34) Mokari, T.; Rothenberg, E.; Popov, I.; Costi, R.; Banin, U. *Science* **2004**, *304*, 1787−1790.
(35) Kudera, S.; Carbone, L.; Casula, M. F.; Cingolani, R.; Falqui, A.; Snoeck, E.; Parak, W. J.; Manna, L. *Nano Lett.* **2005**, *5*, 445−449.

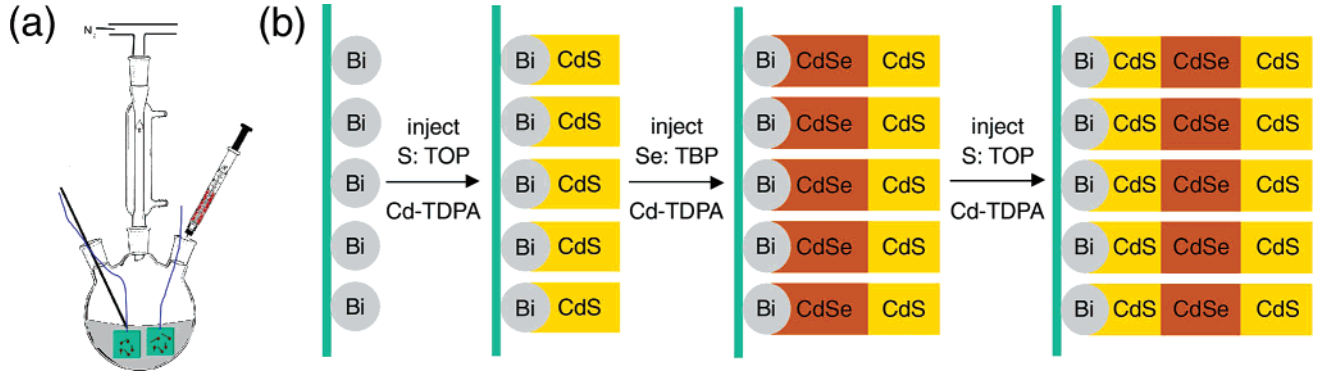

Figure 1. Synthesis of axial nanorod heterostructures. (a) Schematic of the solution reaction setup. (b) Bismuth nanocrystal catalysts nucleate and direct 1D nanorod heterostructure growth with the catalysts remaining at the terminus of the nanorods.

tors,[22] light-emitting diodes,[23] and various quantum-dot geometries based on *p-n* and *p-n-p* junctions.[24]

Axial compositional modulation in nanorods and nanowires is typically achieved using either of the two synthetic methods developed over the past few years: the nanocrystal-assisted growth of III−V and IV nanorod heterostructures[21−29] by the vapor−liquid−solid (VLS) mechanism[36] and the noncatalytic growth of colloidal nanocrystal heterostructures in solution.[31−35] Unfortunately, neither of these two approaches has successfully been applied to controllably synthesize cadmium chalcogenide (CdE) axial heterostructures. The VLS method fails because the reaction temperature (700−900 °C) required for nanowire growth is much higher than the alloying temperature (∼400−500 °C) of the CdE materials[37−39] resulting from their small mixing enthalpies.[40] Lower reaction temperatures employed in the solution method circumvent this alloying problem. Previous studies have shown, however, that only a limited number of linear II−VI configurations can be prepared using the solution method (for example, the synthesis of CdS/CdSe/CdS nanorod heterostructures could not be achieved).[31−33] Moreover, the short length of each segment (normally a few tens of nanometers) imposes challenges in incorporating these solution-grown heterostructures into electrical and optical devices.

Here, we report a new nanocrystal-catalyzed solution method to make axial CdE nanorod heterostructures with predesigned compositional modulation. This method is built upon the recent developments in solution-phase metal-catalyzed nanowire synthesis[41−46] where metal nanocrystals[47,48] were used to grow semiconductor nanowires by way of a solution−liquid−solid (SLS) growth process.[43] In the present study, metal nanocrystal catalysts in a substrate-bound form[46] are introduced into an organic solution containing the reactive precursors (Figure 1a), resulting in nanorods and wires grown on a substrate. The substrates with catalyst-bound nanorods are then transferred to subsequent reaction flasks to grow nanorod heterostructures with linear composition modulation (Figure 1b). In principle, this approach can be successfully implemented if a nanocrystal catalyst is found that is suitable for growth of the different heterostructure components under similar reaction conditions. Bismuth (Bi) nanocrystals are found to meet this requirement for CdE heterostructure growth, successfully yielding Bi/CdS/CdSe, Bi/CdSe/CdS, and Bi/CdS/CdSe/CdS with the length of each segment reaching hundreds of nanometers.

Electron microscopy and diffraction studies show that both CdSe and CdS segments exhibit the wurtzite (hexagonal) crystal structure with <5% stacking faults, with growth along the [002] direction. Importantly, the junctions between CdSe and CdS sections exhibit an epitaxial interface and the alloy-free localization of Se and S within each section. Electrical transport measurements show that devices incorporating individual CdSe/CdS nanorod heterostructures exhibit rectifying behavior, demonstrating that the compositional modulation can successfully encode a device function that cannot be achieved with a single-component nanostructure.

Experimental Section

Chemicals. Cadmium oxide (CdO, 99.99%), tributylphosphine (TBP, 97%), trioctylphosphine (TOP, 90%), tri-*n*-octylphosphine oxide (TOPO, 99%), anhydrous hexanes, sulfur (S, 99.99%), and selenium (Se, 99.999%) powder were purchased from Aldrich. Bismuth spheres (Bi, 99.999%) and *n*-tetradecylphosphonic acid (TDPA, 98%) were purchased from Alfa Aesar. Acetone and 2-propanol were purchased from VWR. Chromium-plated tungsten rods and tungsten boats were purchased from RD Mathis Company. Si, InP, InAs, and GaAs wafers were purchased from University Wafer.

Synthesis of Cadmium Precursors. CdO (0.0048 g, 0.037 mmol) and TDPA (0.0214 g, 0.074 mmol) with 5 g of TOPO were loaded into a 50-mL reaction flask and then heated under nitrogen flow. The mixture turned clear at around 300 °C in TOPO solution. After the solution was kept at the dissolving temperature for 30−60 min, it was allowed to cool to room temperature under nitrogen flow. A white solid product was obtained and was kept in a glove box under a nitrogen atmosphere. For the CdS synthesis, the Cd/TDPA complex, after aging for at least 48 h, was used directly without further purification steps. For the CdSe synthesis, the Cd/TDPA complex was used with or

(36) Wagner, R. S.; Ellis, W. C. *Appl. Phys. Lett.* **1964**, *4*, 89−90.
(37) Halsall, M. P.; Nicholls, J. E.; Davies, J. J.; Cockayne, B.; Wright, P. J.; Cullis, A. G. *Semicond. Sci. Technol.* **1988**, *3*, 1126−1128.
(38) Parbrook, P. J.; Wright, P. J.; Cockayne, B.; Cullis, A. G.; Henderson, B.; O'Donnell, K. P. *J. Cryst. Growth* **1990**, *106*, 503−509.
(39) Wright, P. J.; Cockayne, B.; Jones, A. C.; Orrell, E. D.; O'Brien, P.; Khan, O. F. Z. *J. Cryst. Growth* **1989**, *94*, 97−101.
(40) Wei, S. H.; Zhang, S. B.; Zunger, A. *J. Appl. Phys.* **2000**, *87*, 1304−1311.
(41) Yu, H.; Li, J. B.; Loomis, R. A.; Gibbons, P. C.; Wang, L. W.; Buhro, W. E. *J. Am. Chem. Soc.* **2003**, *125*, 16168−16169.
(42) Grebinski, J. W.; Hull, K. L.; Zhang, J.; Kosel, T. H.; Kuno, M. *Chem. Mater.* **2004**, *16*, 5260−5272.
(43) Trentler, T. J.; Hickman, K. M.; Goel, S. C.; Viano, A. M.; Gibbons, P. C.; Buhro, W. E. *Science* **1995**, *270*, 1791−1794.
(44) Holmes, J. D.; Johnston, K. P.; Doty, R. C.; Korgel, B. A. *Science* **2000**, *287*, 1471−1473.
(45) Yu, H.; Buhro, W. E. *Adv. Mater.* **2003**, *15*, 416−419.
(46) Lu, X. M.; Hanrath, T.; Johnston, K. P.; Korgel, B. A. *Nano Lett.* **2003**, *3*, 93−99.
(47) Yu, H.; Gibbons, P. C.; Kelton, K. F.; Buhro, W. E. *J. Am. Chem. Soc.* **2001**, *123*, 9198−9199.
(48) Grebinski, J. W.; Richter, K. L.; Zhang, J.; Kosel, T. H.; Kuno, M. *J. Phys. Chem. B* **2004**, *108*, 9745−9751.

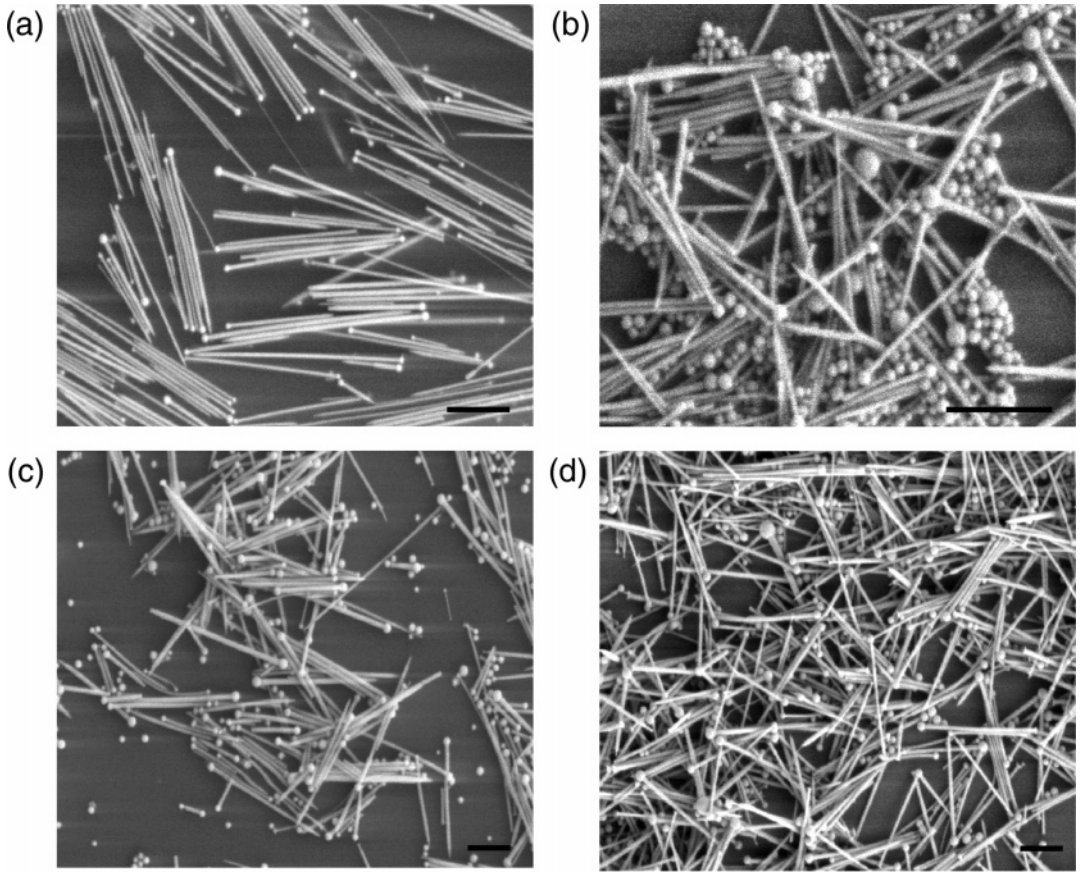

Figure 2. SEM images of the single-component nanorods grown on substrates with different thicknesses of bismuth. Nanorods of (a) CdSe grown from a 4-nm Bi layer, (b) CdS from a 4-nm Bi layer, (c) CdSe from an 8-nm Bi layer, and (d) CdS from a 15-nm Bi layer. All scale bars represent 500 nm.

without aging. Unless indicated otherwise, Cd/TDPA will always refer to the *aged* complexes in this article.

Preparation of Bi-Covered Substrates. Si/SiO_2 and III−V wafers were cleaned with acetone and 2-propanol before being loaded into a high vacuum thermal evaporator. A few nanometers (4, 8, or 15 nm) of Bi were thermally evaporated on top of a thin (2.5−5 nm) primer layer of Cr. The Bi-covered substrates were kept in a nitrogen glove box.

Synthesis of CdSe and CdS Nanorods on Substrates. The Bi-covered substrates were cut into ~0.25 in. × 0.25 in. chips and tethered to poly(tetrafluoroethylene) (PTFE) threads before being loaded into a 50-mL three-neck round-bottom flask containing Cd/TDPA (Figure 1a). The reaction setup and scheme are shown in Figure 1. The flask was heated to 270 °C, then 0.01−0.02 mL of 25 wt % Se/TBP solution (or 0.15 mL of 8 wt % S/TOP solution for CdS reaction) was injected into the Cd/TDPA TOPO solution. The chips were retrieved from the solution by pulling the PTFE threads 3−10 min after the injection. The flask was allowed to cool to room temperature. The chips were washed with hexanes to remove residual TOPO and unreacted trace chemicals. The CdSe or CdS nanorods with Bi catalyst particles attached to one end (Bi/CdSe or Bi/CdS) were found on the chips.

Synthesis of Nanorod Heterostructures. The chips with Bi/CdSe (or Bi/CdS) nanorods were rinsed with anhydrous hexane and dried before being placed in a new flask with Cd/TDPA. The same procedure as mentioned above was carried out. After being rinsed with hexanes, Bi/CdS/CdSe (or Bi/CdSe/CdS) nanorod heterostructures were found on the chips. To make Bi/CdS/CdSe/CdS heterostructures, chips with Bi/CdSe/CdS were used for another reaction round.

Characterization of Samples. The morphology of the CdE nanorods and heterostructures was analyzed with a LEO 982 field-emission scanning electron microscope (SEM) and a JEOL 2010 transmission electron microscope (TEM) with scanning-mode TEM (STEM) imaging and energy-dispersive X-ray (EDX) mapping capabilities. The SEM imaging was performed on the as-synthesized product on chips. Samples for TEM imaging were made by depositing a hexane solution of nanorods (prepared by sonication of as-synthesized chips in hexane) onto holey carbon 300 mesh copper grids (Structure Probe, Inc.).

Fabrication of Electrical Devices. Devices incorporating individual nanorod heterostructures were fabricated by first depositing a hexane solution of nanorods onto a degenerately doped silicon wafer coated with 300-nm-thick oxide (see Figure 6 inset for device image). Individual nanorods were located with the aid of prepatterned alignment marks. Source and drain electrodes were defined using electron beam lithography, followed by thermal evaporation of Ti (4 nm) and Au (110 nm), and liftoff. The doped silicon substrate was used as a gate electrode.

Results

The morphology of the reaction product was examined using SEM and TEM. Figure 2 shows representative SEM images of single-component nanorods, illustrating that the reaction produces straight CdE nanorods with Bi catalysts attached to one end. The diameters of CdSe nanorods range from 20 to 130 nm depending on the thickness of the evaporated Bi layer (Table 1), and the lengths vary from 500 nm to 3 μm. The CdS nanorod diameters range from 15 to 80 nm (Table 1), and the lengths vary from a few hundred nanometers to 1 μm. There are also a few thin (diameter $\leq$ 20 nm) curly nanowires with lengths reaching tens of micrometers on the substrates and in the reaction solution (see the Discussion for more details).

Representative SEM and TEM images of nanorod heterostructures with two or three components are shown in Figure 3. The CdSe sections always have larger diameters than the

Table 1. Size Distribution of Bi Nanocrystals, CdSe Nanorods, and CdS Nanorods Based on Bi Film Thickness

thickness of Bi layer (nm)	4	8	15
diameter distribution of Bi nanocrystals (nm)	45 ± 20	75 ± 20	108 ± 34
diameter distribution of CdSe nanorods (nm)	30 ± 10	49 ± 16	96 ± 30
diameter distribution of CdS nanorods (nm)	26 ± 8	41 ± 11	61 ± 25

CdS sections grown from the Bi catalysts with the same size, and the heterostructure components could thus be distinguished with SEM even without elemental analysis.

EDX spectrometry was used to examine the local atomic composition of the heterostructures. The resulting line profiles of two-component nanorod heterostructures obtained in STEM mode are illustrated in Figure 4. These elemental line scans confirm the presence of Cd throughout the whole structure, while S and Se appear only locally in the CdS and CdSe segments of the heterostructures, respectively. The line scans show a gradient over a length scale of 20−30 nm. (This could be most accurately determined from Figure 4b, which has a 2-nm scanning interval.) This provides an upper limit for the width of the junction, since it is comparable to the spatial resolution of the instrument determined by the spot size of the scanning electron beam (4−6 nm) and the electron beam drift.

Crystal structures of the nanorods and nanorod heterostructures were determined by electron diffraction and powder X-ray diffraction (see Supporting Information for the diffraction data). Figure 5a shows a TEM image and selected area electron diffraction (SAED) patterns obtained from a representative Bi/CdS/CdSe nanorod. The SAED patterns were indexed to a wurzite crystal structure for both CdSe and CdS segments whose growth directions are parallel to the [002] direction. Figure 5b shows a high-resolution TEM image of the junction of the same nanorod heterostructure with clear lattice fringes, confirming the epitaxial growth of the two CdE components and the material's high crystallinity. The SAED patterns at the heterojunction (Figure 5b inset) clearly show pairs of diffraction peaks along the different lattice directions and suggest that the CdS/CdSe interface is formed without alloying.

Single-nanorod transistor devices were fabricated using either Bi/CdS, Bi/CdSe, or the bilayer Bi/CdS/CdSe. All electrical measurements on these devices were carried out at room temperature and in the dark, due to the significant dependence of the conductance of these materials on light. Figure 6 shows the typical current−voltage ($I-V$) curves for these devices. The CdSe devices exhibited a symmetric $I-V$ characteristic with negligible current at moderate biases and a sharp increase in current above 5 V. Measurements of CdS nanowire devices showed linear $I-V$ curves with a resistance on the order of 1 kΩ and an *n*-type dependence on the gate voltage. Devices incorporating individual CdS/CdSe nanorods had rectifying $I-V$ curves, in which forward bias corresponds to the application of negative voltage to the electrode contacting CdS.

Discussion

Previous studies of vapor-phase synthesis have demonstrated successful 1D growth of CdSe and CdS nanowires with the assistance of Au nanocrystals.[11] The effort to synthesize axial nanorod heterostructures of II−VI semiconductors via the VLS

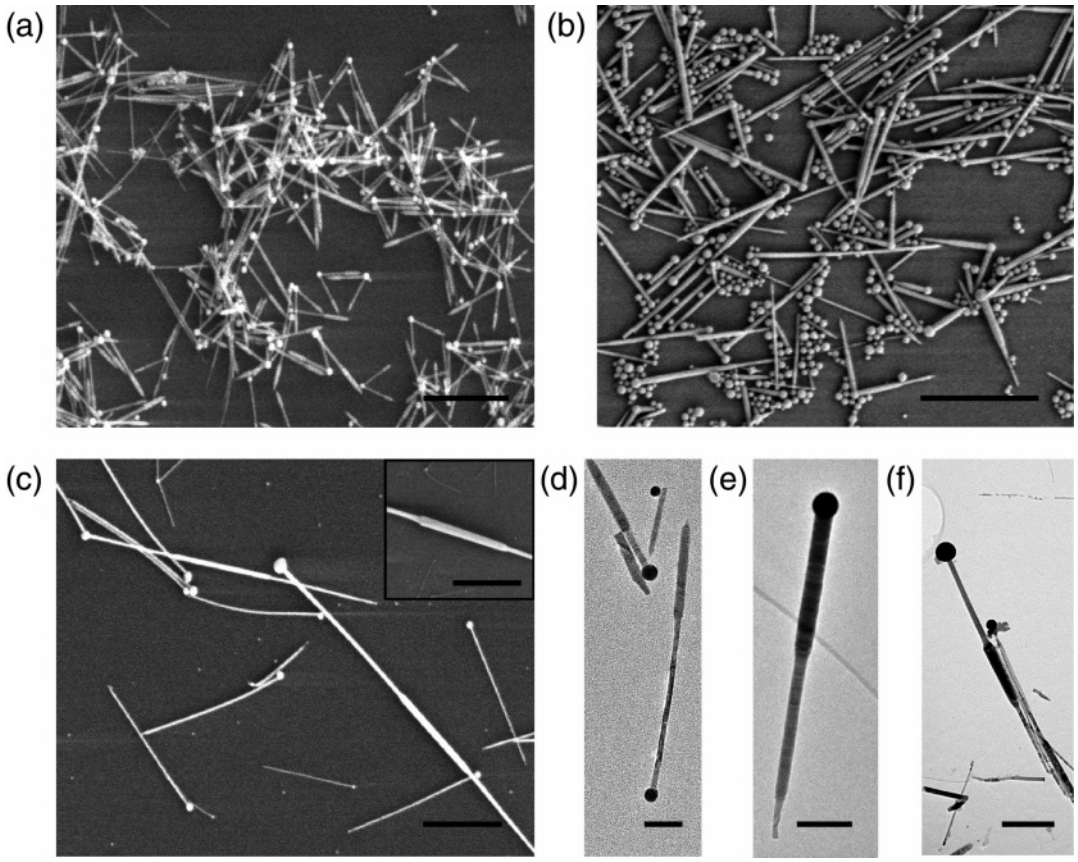

Figure 3. SEM and TEM images of nanorod heterostructures. (a) and (d) Bi/CdS/CdSe with yield ∼100%. (b) and (e) Bi/CdSe/CdS with yield ∼30%. (c) and (f) Bi/CdS/CdSe/CdS. Scale bars represent 1 μm in (a)−(c) and (f) and 200 nm in (d) and (e).

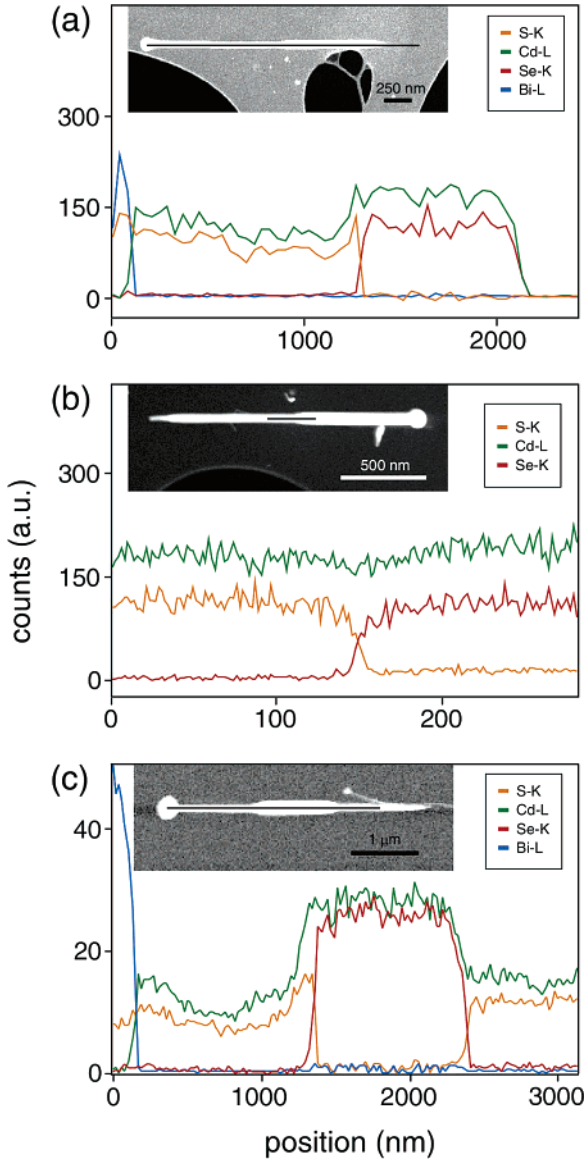

Figure 4. EDX spectrometry line scans of nanorod heterostructures showing the change of composition as a function of the position of detection. Shown are line profiles of the composition through (a) a Bi/CdS/CdSe heterostructure scanned with a 44-nm interval, (b) Bi/CdSe/CdS heterostructure scanned with a 2-nm interval, and (c) Bi/CdS/CdSe/CdS heterostructure scanned with a 20-nm interval. Insets: STEM dark field images of the heterostructures.

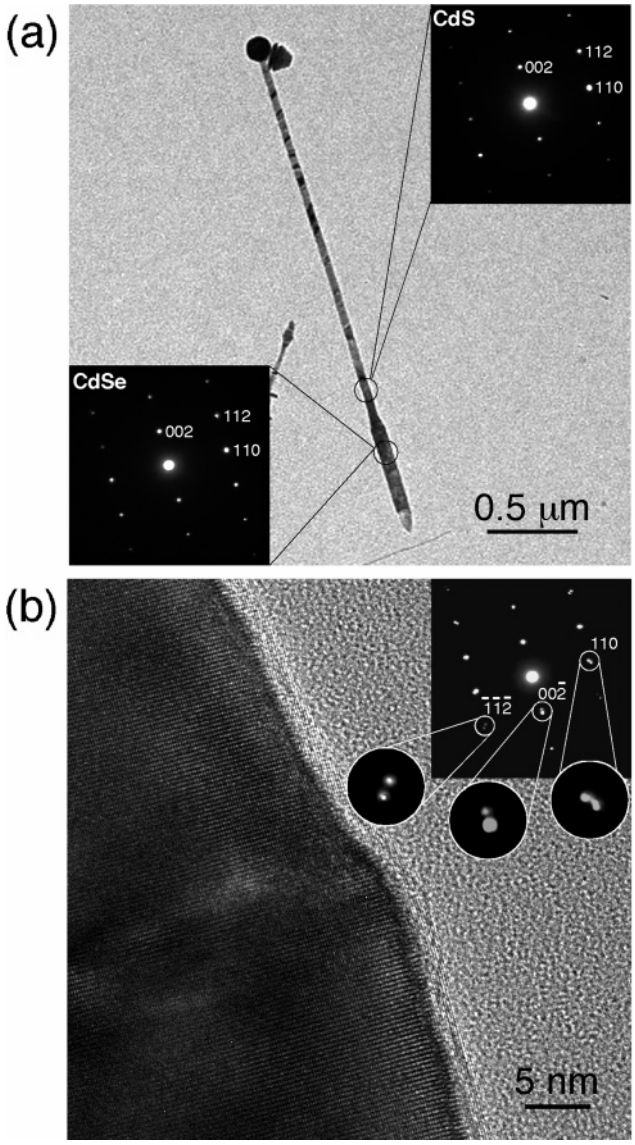

Figure 5. CdS/CdSe nanorod junctions. (a) TEM image of a Bi/CdS/CdSe nanorod heterostructure. Insets: SAED patterns of CdSe and CdS sections showing growth along the [002] lattice direction in the [2$\bar{2}$0] zone axis. (b) High-resolution TEM image of the CdS/CdSe junction of the same nanorod. Inset: SAED of the junction showing a splitting of diffraction peaks of [110], [$\bar{1}$1$\bar{2}$], and [00$\bar{2}$] lattice directions in the [2$\bar{2}$0] zone axis.

method was nevertheless unsuccessful, largely due to the low alloying temperature of II−VI compounds. Bismuth nanocrystals have recently been demonstrated as an ideal catalyst to assist 1D growth of CdSe nanowires in solution at relatively low temperatures based on the SLS mechanism.[41,42] Figures 2 through 5 demonstrate that Bi nanocrystals are also good catalysts for growing CdS nanorods and CdE nanorod heterostructures under similar reaction conditions.

In contrast to the previous studies where Bi nanocrystals synthesized using a chemical method[47,48] were used in solution-phase synthesis,[41,42] a thin layer of bismuth deposited on a substrate was used to form catalyst particles in our reactions. The main advantage of using substrate-bound catalyst particles is that massive purification and reconcentration procedures for reaction products[8−10,31−33,41,42] are not necessary during the transfer of nanorods from one reaction to another. The thin layer of Bi forms Bi nanocrystals at the reaction temperature due to its low melting point (271 °C). Most of the reaction products were found on substrates, with very few Bi-bound CdE nanorods found in the TOPO solution (free-standing nanocrystal byproducts were not found in the solution, most likely because the low concentration of Cd precursor used in these reactions prevents nucleation of nanocrystals without catalyst assistance). It should be noted that the Cr underlayer is critical for the adhesion of the nanocrystals to the substrates. When Bi is the only material evaporated on the substrates, almost no Bi nanocrystals or nanorods were found on the substrates after the reactions, but they were instead dispersed in solution. Substrates such as Si/SiO_2, InP, InAs, and GaAs were used to test the effect of different substrates, without any significant variation in the results.

Because the growth of nanorods is based on the SLS mechanism,[43] the morphology of the products depends on several factors: the size of the nanocrystals, the reaction temperature, and the chemical properties of the precursors. Our

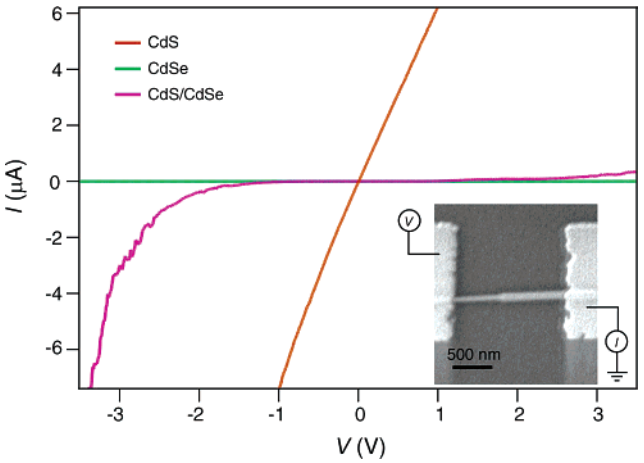

Figure 6. Typical $I-V$ curves for transistor devices incorporating a single CdSe nanorod (green), CdS nanorod (orange), or CdSe/CdS bilayer nanorod (purple). Inset: SEM image of bilayer nanorod device.

study demonstrates that the morphology of the reaction product can be tuned from long nanowires (aspect ratio ≥ 50) to short nanorods (aspect ratio ~3−40) by rationally varying the reaction conditions. For example, formation of thin, curly, and long CdS and CdSe nanowires (up to tens of micrometers) is observed when the reaction temperature is lowered to 240 °C. This is probably due to a smaller saturation concentration of precursors in bismuth nanocrystals caused by lower temperature. The aging of Cd/TDPA is also critical to the morphologies of CdS nanostructures. When freshly made Cd/TDPA is used, long nanowires are formed instead. We propose that the fresh Cd/TDPA complex is less stable and thus more reactive toward the S precursor, decreasing the effective saturation concentration of Cd and S in Bi nanocrystals. The aging of Cd/TDPA was not as critical for the CdSe nanostructure growth, probably because of the higher chemical stability of the Se precursor compared to the S precursor and/or the higher saturation concentration of the Cd/Se mixture in Bi.

The nanorod morphology of CdE components is a key factor in the successful growth of heterostructures. In our reaction scheme, the axial heterostructures formed only when short nanorods were used as starting materials. When long thin nanowires were used instead, heterostructures were not observed after the subsequent reaction. This observation can be attributed to two factors. First, the Bi nanocrystals are covered by the dense "net" of curly long wires from the first reaction, preventing the precursors from reaching the catalysts in the subsequent reaction. Second, the thin nanowires have larger surface areas than the short nanorods and provide more surface nucleation sites that can compete with the catalyst particles.

The average diameter of CdS nanorods is always smaller than that of CdSe nanorods grown from the same substrates (the dispersion of the diameters of Bi nanocrystals and CdE nanorods is as large as tens of nanometers because the bismuth nanocrystals are formed just by the melting of a thin metal film). Also, the diameter of the CdS component is always smaller than that of the CdSe component from the same catalyst. The different average diameters of CdS and CdSe segments may originate from the smaller saturation concentration of CdS in Bi compared to CdSe or from different surface tensions of the liquid CdS/Bi and CdSe/Bi mixtures.

In the Bi-catalyst-assisted growth reported here, CdE nanorods grow very fast once the S or Se precursor is injected, and the length of nanorods can thus reach up to several micrometers within a few minutes. The accurate control over the length of nanorods was difficult, however, because the shortening of the reaction time only resulted in a decrease in rod density. These observations suggest that the initial formation of an interface between the liquid (Bi catalyst) phase and the solid (CdE nanorod) phase is the rate-limiting step of our reactions.

All the nanorods examined have stacking faults (<5%) regardless of their diameters, as observed previously for nanostructures with zinc-blende-wurzite polytypism.[8−10,31,32,42,49] A small portion of the nanorods had branches as shown in Figure 2b, again due to the low energy difference of the two crystal structures.[49] In a few cases, more than one nanorod grew from a single Bi nanocrystal (Figure 2b) especially when the size of the Bi nanocrystals approached ~100 nm.

It should be clearly mentioned that the growths of CdS from Bi/CdSe and CdSe from Bi/CdS were not equally favored. The latter is found to be more difficult, resulting in lower yields for heterostructures. Specifically, the heterostructure yield of the first reaction was almost 100% as shown in Figure 3a, whereas the yield for the latter reaction was around 30% as shown in Figure 3b. The reason for this yield difference is not clear at present and requires further investigation.

The shape of the dark state $I-V$ curve for the CdSe nanorod device is consistent with the formation of back-to-back diodes due to the Schottky barrier between CdSe and Ti/Au. On the other hand, transistor devices incorporating individual CdS nanorods exhibited clear ohmic behavior with an *n*-type dependence on the gate voltage. This *n*-type behavior is consistent with the presence of anion vacancies observed in bulk and thin-film samples of CdS.[50,51] With the measurements on the single-component nanorod devices in mind, the rectifying $I-V$ curve for the bilayer devices can be attributed to the rectifying nature of the *n*-type Schottky barrier at the CdSe/metal interface, while the CdS/metal contact remains ohmic.

Conclusions

We have successfully demonstrated an SLS approach for making CdS and CdSe nanorods and nanorod heterostructures with controlled sequences of these two materials. Our approach combines the merits of solution chemistry (lower reaction temperature and more flexibility in processing) with those of VLS growth (anisotropic growth and the easy purification of substrate-bound products). This general approach should be useful for the synthesis of other colloidal nanorods with built-in heterojunctions.

Acknowledgment. This work was supported by the National Science Foundation and the Packard Foundation. We thank Grace Jhe for helping to synthesize cadmium precursors, and Dr. Y. J. Doh, Dr. D. Bell, and Dr. Y. Lu for scientific discussions and technical assistance.

Supporting Information Available: X-ray diffraction pattern of nanorod heterostructures in Figure S1. This material is available free of charge via the Internet at http://pubs.acs.org.

JA066243U

(49) Yeh, C. Y.; Lu, Z. W.; Froyen, S.; Zunger, A. *Phys. Rev. B* **1992**, *46*, 10086−10097.
(50) Gersten, J. I.; Smith, F. W. In *The Physics and Chemistry of Materials*; Wiley & Sons: New York, 2001; p 417.
(51) Streetman, B. G.; Banerjee, S. In *Solid State Electronic Devices*; Prentice Hall: Upper Saddle River, NJ, 2000; p 392.